Microstructural Evolution and Mechanical Properties of $Ni_{57}Nb_{33}Zr_5Co_5$ Metallic Glass

Siriwan Dulnee[a]*, Claudio Shyinti Kiminami[a], Piter Gargarella[a], Michael Joseph Kaufman[b]

[a]*Departamento de Engenharia de Materiais, Universidade Federal de São Carlos, Rodovia Washington Luís, km 235 SP-310, 13565-905, São Carlos, SP, Brazil*
[b]*Department of Metallurgical and Materials Engineering, Colorado School of Mines, 80401, Golden, CO, USA*

The $Ni_{57}Nb_{33}Zr_5Co_5$ metallic glass is a promising alloy for bipolar plates in proton exchange membrane fuel cells. It is important to know which phase forms in this alloy under different cooling rates in order to understand its influence on the thermal stability and mechanical properties. In this work, melt-spun ribbons and rod samples with 1, 2 and 3 mm diameters were prepared and their phase formation, microstructure and mechanical properties were investigated by X-ray diffraction, differential scanning calorimetry, optical microscopy, scanning electron microscopy and microhardness. It is found that a completely crystalline structure forms in the lower cooling rate samples (2 and 3 mm diameter rods) with the presence of the equilibrium phases $Ni_3(Nb,Zr)$ and Nb_7Ni_6 as primary phases or as a very fine eutectic structure, while a fully glassy structure is attained in the samples with the highest cooling rate (ribbons). For the sample with an intermediate cooling rate (1 mm diameter rod), polymorphically crystals of an unknown metastable phase with spherical morphology precipitate in the glassy matrix with virtually the same composition as the matrix. The 2 mm diameter sample exhibits higher hardness than the other samples, which is attributed to its very fine eutectic colonies.

Keywords: *metallic glasses, proton exchange membrane fuel cells, bipolar plates, Ni-based alloys*

1. Introduction

Ni-based metallic glasses have generated substantial recent interest for their potential use as bipolar plates in Proton Exchange Membrane Fuel Cells (PEMFCs)[1-3], primarily due to their higher corrosion resistance, compared with conventional stainless steels (i.e., 316L, SUS316L), their high mechanical strengths, and their easy of processing in the supercooled liquid state. According to Hu et al.[4], among the Ni-based metallic glasses, the $Ni_{57}Nb_{33}Zr_5Co_5$ alloy shows high glass forming ability (GFA) and high corrosion resistance in 6 M HCl, open to air at room temperature. While Inoue et al.[1] have investigated the use of Ni-based glasses as bipolar plates under simulated conditions of PEMFCs, no studies exist on the use this particular alloy under PEMFC working conditions and no systematic investigation of the correlation between phase formation, microstructure and properties of this $Ni_{57}Nb_{33}Zr_5Co_5$ metallic glass have been reported.

In order to control and improve the properties of bipolar plates, an investigation of the influence of cooling rate on the phase formation and microstructure of the $Ni_{57}Nb_{33}Zr_5Co_5$ metallic glass composition was initiated with the goal of characterizing its potential use as bipolar plates in PEMFCs.

In this work, the characteristics of phase formation and microstructure, which may affect the thermal stability and mechanical properties of samples have been determined, for different rapidly solidified $Ni_{57}Nb_{33}Zr_5Co_5$ samples (i.e., melt-spun ribbons and chill-cast rods of 1, 2 and 3 mm diameter) using X-ray diffraction (XRD), differential scanning calorimetry (DSC), optical microscopy, scanning electron microscopy (SEM) and microhardness.

2. Experimental Procedure

Pure elements (> 99.9% purity) were used to prepare ingots of the $Ni_{57}Nb_{33}Zr_5Co_5$ alloy. All elements were formerly etched by using acid solutions (i.e., 36% CH_3COOH + 60% HNO_3 +4% HF, 40% HCl + 20% HNO_3 + 40% HF, 47.6% H_2O + 47.6% HNO_3 + 4.8% HF, and 70% H_2O + 30% HCl for Ni, Nb, Zr, and Co, respectively)[5]. Thereafter, they were melted and homogenized using a Bühler arc melter model AM in a Ti-gettered Ar atmosphere. Negligible weight loss occurred during the melting process (~ 0.6 wt.%).

The ingots were then used to cast rod samples by using a compact arc melter MAM-1 supplied by Edmund Bühler GmbH also in a Ti-gettered Ar atmosphere. To prepare rods with 1, 2, and 3 mm diameter and 35 mm length, the Cu-mold suction casting process was employed. Ribbons were produced using a melt spinner supplied by Edmund Bühler GmbH. The Cu wheel frequency was 70 Hz, the difference of pressure for injection was 200 mBar, and the distance from the crucible to the wheel was around 0.5 mm. The injection temperature was 1300 ºC, 100ºC higher than the liquidus

* e-mail: s.dulnee@gmail.com

temperature measured by differential scanning calorimetry (DSC, 1200ºC).

The microstructure and phase formation of the samples were analyzed by X-ray diffraction (XRD) using a Siemens D5005 diffractometer with Cu-Kα radiation, optical microscopy (Olympus BX41M-LED) and scanning electron microscopy (FEI Inspect S 50 with a coupled EDX system). The thermal stability of the different samples were investigated by DSC using a NETZSCH DSC model 200F3 Maia with a heating/cooling rate of 20/40 K/min, respectively. The mechanical properties were evaluated by Vickers microhardness measurements using a HMV-2000 SHIMADZU microhardness tester and a Vickers pyramid-shaped diamond indenter, under 300 g of loading.

3. Results and Discussion

The XRD results for the ribbon and rods with 1, 2 and 3 mm diameters are shown in Fig. 1. As can be seen, the 2 and 3 mm diameter rods exhibit sharp Bragg peaks, whereas the 1 mm diameter rod exhibits an almost fully amorphous structure confirmed by a presence of a broad diffraction peak around 42º and a lower intensity sharp diffraction peak around 31º. The ribbon presents a complete amorphous structure with a broad diffraction peak also around 42º.
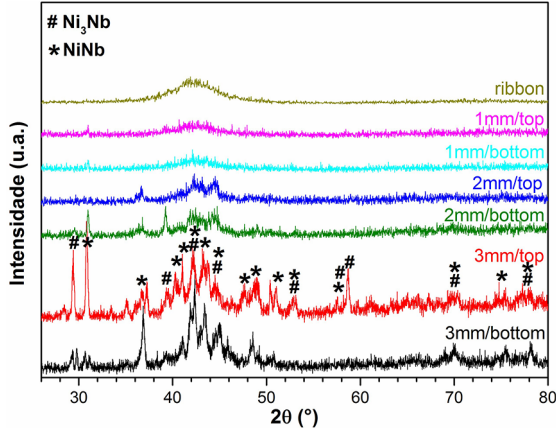
Figure 1. XRD results of the bottom and top parts of each rod (1, 2 and 3 mm diameters) and of ribbon.

A higher amount of amorphous phase forms in samples solidified under higher cooling rates. The cooling rate applied to prepare the samples can be calculated using equation 1[6]:

$$\dot{\mathrm{T}} = \frac{dT}{dt} = \frac{K(T_m - T_o)}{CR^2} \quad (1)$$

where K corresponds to the thermal conductivity of the samples, T_m and T_o are respectively melting and room temperatures, C is the thermal capacity per unit of volume, and R is the thickness of the plate. It can be seen that the

cooling rate is inversely proportional to the diameter/thickness of the sample[6], which agrees with the results since diameters equal or smaller than 1 mm show only glassy phase, while crystalline phases of the hexagonal (Ni,Co)$_3$(Nb,Zr) and rhombohedral (Ni,Co)(Nb,Zr) are formed in larger diameter rod samples. These phases are expected from the equilibrium phase diagram[7]. Further, small different XRD patterns between the bottom and top parts of 3 mm samples have been observed which might be due to a difference in cooling rate at the bottom and top part of the mold. While the same phases were identified in both sample regions, some differences in peak intensity are noticed which might be related to the differences in texture.

Glass transition and crystallization temperatures are given by the two exothermic peaks clearly seen for the ribbons and the 1 mm diameter rod (Fig. 2). The onset glass transition temperature (T_g) and crystallization temperature (T_x) of ribbon and 1 mm diameter rod are 883±2 and 928±2 K and 879±2 and 920±2 K, respectively. DSC profiles shown in Fig. 2 provide evidence to confirm that the 1 mm diameter rod is partially crystalline. Specifically, the crystallization peak area for the 1 mm diameter specimen is 73.2-95.2 % that is the 100% glassy phase of the melt-spun ribbon. No crystallization or glass transition was observed for the 2 and 3 mm diameter rods consistent with them being fully crystalline as expected from the XRD patterns. The thermal parameters (T_g, T_x, and ΔT_x) obtained for the 1 mm diameter rod are slightly different compared with the ribbon, probably due to the presence of crystals in the former sample (Fig. 2).
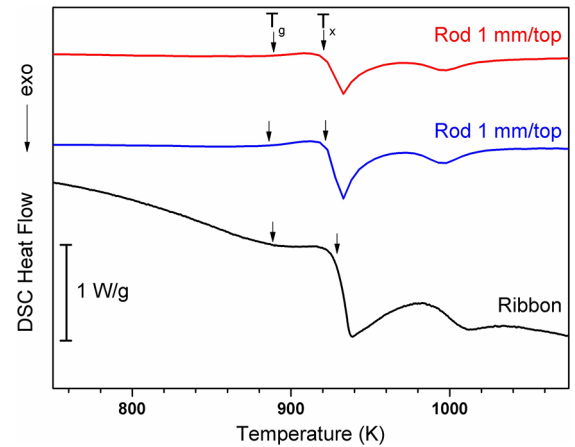
Figure 2. DSC results of 1 mm diameter rod (top and bottom) and ribbon.

An SEM image of the 1 mm rod sample (Fig. 3a) appears to be fully glassy although there were occasional small spherical crystals near the surface of the sample that were not identified (Fig. 3(a)). For the 2 mm diameter rod, a fine eutectic of (Ni,Co)(Nb,Zr) and (Ni,Co)$_3$(Zr,Nb) (Fig. 3b) was observed along with a coarser eutectic structure and some primary (Ni,Co)$_3$(Zr,Nb) phase identified by EDS (Fig. 3c)
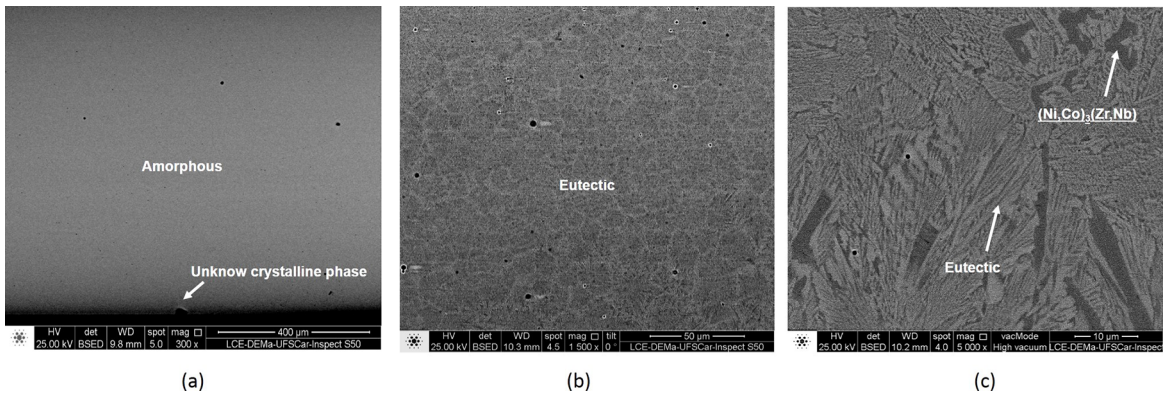
Figure 3. SEM images of: (a) 1 mm diameter rod (top) sample and (b) 2 mm diameter rod (bottom). It suggests the presence of a very fine eutectic formed by (Ni,Co)(Nb,Zr) and (Ni,Co)$_3$(Zr,Nb); (c) 3 mm diameter rod (bottom). The primary (Ni,Co)$_3$(Zr,Nb) phase is formed in a eutectic (Ni,Co)(Nb,Zr)/(Ni,Co)$_3$(Zr,Nb) matrix.

is formed in 3 mm diameter. SEM images further confirm that crystalline phase formed in the 2 and 3 mm diameter samples consistent with the XRD and DSC results.

In order to compare the mechanical properties of the rods, micro hardness tests were conducted and the results are summarized in Table 1. The hardness values of the 1, 2 and 3 mm diameter rods are about 800, 1000 and 815 HV0.3, respectively, corresponding to average yield strength values around 2611, 3305 and 2693 MPa estimated by using the relation σ_s = HV/3, where σ_s is given in kgf/mm^2 [8]. These values are in accordance with the values of rapidly-solidified Ni-based alloys reported in the literature[4]. A greater hardness in the 2 mm rod corresponds to its fine eutectic structure (Fig. 3b).

Table 1. Vickers microhardness results of the top and bottom region of 1, 2 and 3 mm diameter rods.

Sample	HV0.3
Rod 1 mm diameter/top	795±36
Rod 1 mm diameter/bottom	802±12
Rod 2 mm diameter/top	1006±68
Rod 2 mm diameter/bottom	1016±33
Rod 3 mm diameter/top	832±55
Rod 3 mm diameter/bottom	815±52

Further, cracks were formed around the indentation in the 2 mm rod (Fig. 4a), suggesting a low fracture toughness. The critical stress intensity factor, K_{IC}, can be estimated using the Palmqvist cracks observed around the indentation (Fig. 4a) and using the following equation[9]:

$$\left(\frac{K_{IC\varphi}}{H_a^{1/2}}\right)\left(\frac{H}{E_\varphi}\right)^{2/5} = 0.035\left(\frac{l}{a}\right)^{-1/2} \quad (2)$$

where K_{IC} is the Mode I critical stress intensity factor, φ is the constraint factor (≈ 3), H is the hardness (1011 HV0.3), E is the Young's modulus (200 GPa), a is the half diagonal of the Vickers indent (12.12 µm) and l is the length of the
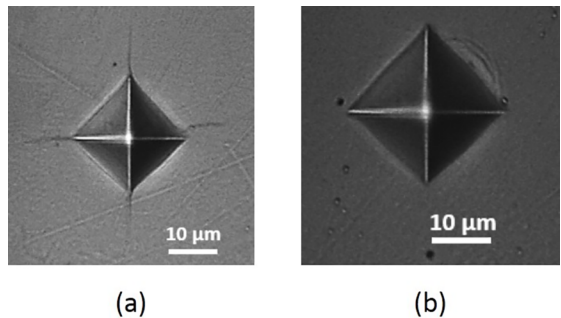
Figure 4. (a) Indentation mark at the 2 mm diameter (bottom part) rod, showing the presence of Palmqvist cracks. (b) Shear bands (SBs) formation around the indentation at the 1 mm diameter rod (bottom). SBs are typically formed during deformation of metallic glasses.

Palmqvist crack (10.35 µm). The value obtained for K_{IC} is 2.25 MPa.m$^{1/2}$ and is in the range of indentation toughness values common in Fe-based and Mg-based metallic glasses[10] and is smaller than the value measured using standard methods (the K_{IC} value of Ni-based crystalline alloys is around 236 MPa.m$^{1/2}$ [11]). Shear bands (SBs) are present near the indentations in the 1 mm glassy rod (Fig. 4b) consistent with the deformation in bulk metallic glasses[12].

4. Conclusions

Among the samples investigated, the Ni$_{57}$Nb$_{33}$Zr$_5$Co$_5$ ribbons exhibit a fully glassy structure with glass transition and crystallization temperatures around 883±2 and 928±2 K, respectively. The lower cooling rate samples (2 and 3 mm diameter rods) exhibit completely crystalline structures with the presence of the equilibrium (Ni,Co)(Nb,Zr) and (Ni,Co)$_3$(Zr,Nb) phases. In the 1 mm diameter sample with an intermediate cooling rate, an almost fully glassy structure (~80% glass) containing small spherical crystals of an unknown phase near the surface was observed. The 2 mm diameter rod had the highest hardness, around 1000 HV0.3, resulting from its fine eutectic mixture of the stable (Ni,Co)(Nb,Zr) and (Ni,Co)$_3$(Zr,Nb).

5. Acknowledgements

6. References

1. Inoue A, Shimizu T, Yamaura SI, Fujita Y, Takagi S, Kimura H. Development of Glassy Alloy Separators for a Proton Exchange Membrane Fuel Cell (PEMFC). *Materials Transactions*. 2005;46(7):1706-1710.

2. Jayaraj J, Kim YC, Seok HK, Kim KB, Fleury E. Development of metallic glasses for bipolar plate application. *Materials Science and Engineering: A*. 2007;449-451:30-33.

3. Thalmaier G, Vida-Simiti I, Vermesan H, Codrean C, Chira M. Corrosion Resistance Measurements of Amorphous Ni40Ti40Nb20 Bipolar Plate Material for Polymer Electrolyte Membrane Fuel Cells. *Advanced Engineering Forum*. 2013;8-9:335-342.

4. Hu HT, Chen LY, Wang XD, Cao QP, Jiang JZ. Formation of Ni–Nb–Zr–X (X = Ti, Ta, Fe, Cu, Co) bulk metallic glasses. *Journal of Alloys and Compounds*. 2008;460(1-2):714-718.

5. Petzow G. *Metallographic Etching: Metallographic and Ceramographic Methods for Revealing Microstructure*. Materials Park: American Society for Metals; 1976.

6. Lin XH, Johnson WL. Formation of Ti-Zr-Cu-Ni bulk metallic glasses. *Journal of Applied Physics*. 1995;78(11):6514.

7. Zeng K, Zeng X, Jin Z. A thermodynamic calculation of the Ni-Nb phase diagram. *Journal of Alloys and Compounds*. 1992;179(1-2):177-185.

8. Dieter GE. *Mechanical Metallurgy*. London: McGraw-Hill; 1988.

9. Niihara K, Morena R, Hasselman DPH. Evaluation of K$_{Ic}$ of brittle solids by the indentation method with low crack-to-indent ratios. *Journal of Materials Science Letters*. 1982;1(1):13-16.

10. Madge SV. Toughness of Bulk Metallic Glasses. *Metals*. 2015;5:1279-1305.

11. MatWeb. *Property Search*. Available from: <http://www.matweb.com/search/PropertySearch.aspx>. Access in: 12/6/2017.

12. Schuh CA, Hufnagel TC, Ramamurty U. Mechanical behavior of amorphous alloys. *Acta Materialia*. 2007;55(12):4067-4109.